ACS OMEGA

http://pubs.acs.org/journal/acsodf

Article

Al-Substituted Tobermorites: An Effective Cation Exchanger Synthesized from "End-of-Waste" Materials

Daniele Malferrari,* Fabrizio Bernini, Dario Di Giuseppe, Valentina Scognamiglio, and Alessandro F. Gualtieri

Cite This: *ACS Omega* 2022, 7, 1694−1702

Read Online

ACCESS | Metrics & More | Article Recommendations | Supporting Information

ABSTRACT: The policies to meet the "zero waste" regime and transition to sustainable circular economy can no longer ignore the use of wastes in place of natural resources, and these daunting and vital societal challenges are nowadays being faced by several nations. The main objective of this work was to search waste materials suitable for a quick and environmentally friendly production of a nanoporous geomaterial able to trap toxic metals at the solid/liquid interface. More specifically, the end-of-waste from the thermal inertization of cement−asbestos and glass powder from domestic glass containers have been employed as sources for the hydrothermal synthesis of a tobermorite-rich material (TRM) successfully tested for the selective removal of Pb^{2+}, Zn^{2+}, Cd^{2+}, and Ni^{2+} from aqueous solutions. The synthesis was carried out in alkaline solution under mild hydrothermal conditions (120 °C) within 24 h. The quantitative phase analyses of the TRM carried out by applying the Rietveld method showed the occurrence of a large amount of well-crystallized 11 Å Al-substituted tobermorites and an amorphous phase and a lower content of aragonite and calcite. Chemical analyses and thermogravimetric measurements coupled with simultaneous evolved gas mass spectrometry highlighted that Al^{3+} for Si^{4+} substitutions in the wollastonite-like tetrahedral chains of tobermorites are balanced by the occurrence of Ca^{2+}, Na^{+}, and K^{+} cations in the interlayer rather than by $(OH)^{-}$ for O^{2-} substitutions in the CaO polyhedra. Time-dependent removal tests clearly indicated that metal cations are selectively adsorbed depending on their concentration in solution. Moreover, the kinetic curves showed that the removal of metals from solution is fast and the equilibrium is almost reached in the first 8 h.

1. INTRODUCTION

One of the main challenges for modern society is to reduce the production of waste and limit the consumption of natural raw materials (NRM) whose availability is increasingly difficult and costs are increasing.[1] At once, the growing awareness for the "environmental issues" has led to the development of environment-friendly, sustainable, and cost-effective industrial processes and, in several countries, new production activities can be launched only if fully integrated within the circular economy regime.[2−5] Nevertheless, these goals are frustrated by the fact that, for a long time, humans will have to live with the hazardous waste produced in the past and the nonhazardous waste generated at a faster rate than their recycling. Two typical examples are asbestos and glass from the recycling of domestic containers.

In countries where asbestos is banned, massive amounts of asbestos-containing materials, especially cement−asbestos slates (CAS), must be removed and disposed.[6] Disposal in landfills cannot be the ultimate solution not only as it conflicts with the directives of the European Commission (2008/98/EC, end-of-waste concept) but also as zero risk of fiber dispersion in air and water in the long run cannot be guaranteed.[7] A very promising alternative to landfill storage is the inertization achieved through thermal treatment as firing of CAS yields an inert fine material, generally referred to as KRY·AS.[7−9] KRY·AS is an end-of-waste and has been proposed as a replacement for NRM in various applications depending on its mineralogical and chemical composition, demonstrating that the thermal inertization and recycling of the product of transformation are an effective solution to the asbestos problem.[10,11]

The separate collection of domestic glass containers (DGC) is a political obligation within many nations and it has progressively increased in the last decades as demonstrated by several national reports.[12−14] Nevertheless, their recovery is

Received: August 5, 2021
Accepted: October 15, 2021
Published: January 4, 2022

Table 1. Elemental Composition (mol/100 g) and Loss on Ignition (LOI, Weight %) at 1100 °C of KRY·AS, Glass Powder, Zeolitic Tuff, KGT, and TRM[a]

	KRY·AS	glass powder	zeolitic tuff	KGT[b]	KGT[c]	KGT[d]	TRM[c]	TRM[d]
Si	0.4139	1.1538	0.8778	0.6562	0.6634	0.6870	0.5715	0.7065
Al	0.0798	0.0557	0.3238	0.0771	0.0759	0.0786	0.0610	0.0754
Fe	0.0341	0.0059	0.0482	0.0255	0.0262	0.0271	0.0207	0.0256
Ti	0.0026	0.0018	0.0054	0.0024	0.0025	0.0026	0.0019	0.0023
P	0.0000	0.0003	0.0008	0.0001	0.0001	0.0001	0.0001	0.0002
Mn	0.0010	0.0007	0.0021	0.0009	0.0011	0.0012	0.0007	0.0009
Mg	0.2363	0.0620	0.0270	0.1772	0.1777	0.1840	0.1526	0.1887
Ca	0.8622	0.1648	0.0794	0.6269	0.6323	0.6444	0.5359	0.6626
Na	0.0083	0.3957	0.0323	0.1308	0.1384	0.1330	0.1591	0.1967
K	0.0062	0.0164	0.1232	0.0118	0.0121	0.0392	0.0098	0.0121
LOI	9.65	2.42	13.94	7.46	6.09	0.00	19.11	0.00

[a]TRM chemical composition is listed here to facilitate the comparison with source materials. [b]Calculated. [c]Experimental. [d]Experimental recalculated as anhydrous.

often frustrated by various aesthetic and technical hindrances which, sometimes, leave landfill disposal as the only solution.[15−18] Typical limiting factors are color heterogeneity, high calcium concentration, not being compatible with fiberglass production, occurrence of metals (in several countries, DGC are collected together with iron and aluminum cans), and, often, the anomalous concentration of lead due to the wrong disposal of crystalware in separate collection which drastically impacts the possible reuse applications.[17,19−21] Although the production of aggregates, concretes, ceramics, and abrasives represents an alternative market with few restrictions, the accumulation of cullet is still much greater than its demand.[15,22−26]

KRY·AS and DGC, in addition to the applications described above, could also be simultaneously used to synthesize nanoporous materials, although this path has not yet been explored significantly. Among them, tobermorite could be an excellent candidate both for its properties and for the low energy consumption necessary for the synthesis. Tobermorite identifies as a group of hydrated calcium silicate minerals with a strong resemblance to 2:1 swelling layer silicates, including the variability of basal spacing with the H_2O content, specific surface area, cation-exchange capacity (CEC), polytypism, and no toxic activity. Each member of the tobermorite group is a family of polytypic compounds which can be described through the order/disorder theory.[27,28] Even though a new nomenclature scheme identifying a tobermorite supergroup was recently proposed,[29] most of the literature describes three main polytypes, plombièrite, tobermorite, and riversideite, according to interlayer spacing (about 14.0, 11.3, and 9.30 Å, respectively) which, in turn, mostly depends on the water content.[30] These polytypes, referring to a more applicative classification criteria, are also known as 14 Å-, 11 Å-, and 9 Å-tobermorite.

Regardless of the polytype, Si forms wollastonite-like tetrahedral chains (the so-called "dreierketten") and can be partially replaced (up to 15%) by Al^{3+} and/or, even if less common, by Fe^{3+} (substituted tobermorites);[31] these heterovalent substitutions are neutralized by a higher Ca content and/or a hydroxyl for oxygen replacements.[28] Ca forms two types of polyhedra, one with a CaO-like structure (seven-fold coordination with oxygen or a hydroxyl) and the other (zeolitic-type) in which Ca^{2+} weakly bonds with a varying number of water molecules. To a first approximation and without considering disorder and polytypism, the ideal structure of tobermorite (Figure SI-1, Supporting Information) is given by a sequence of Ca−Si layers stacked along the *c*-axis; the layers are formed by a central sheet of CaO-like polyhedra coupled on both sides to wollastonite-like tetrahedral chains running along the *b*-axis. The cations solvating water (ideally Ca^{2+} but also Na^+ and K^+) are intercalated between the Ca−Si units in an amount depending on Al^{3+} and Fe^{3+} for Si^{4+} substitutions; moreover, these cations are exchangeable as they are bound through weak hydrogen bonds like those occurring, for example, in smectites.

Although the basic and main technological interest on tobermorite derives from its role as the primary binder in cements and concretes,[32] it is the high CEC of substituted tobermorites that has attracted attention of the applied research, primarily as the adsorbent material for toxic elements and radionuclides.[33−43] Applicative research studies on natural terms are lacking as tobermorite is a relatively rare mineral and exploitable deposits are not known. In contrast, the tobermorite-11 Å, the most abundant and technologically relevant substituted polytype, can be quite easily synthesized under mild hydrothermal conditions from a wide range of Si-, Al-, and Ca-bearing materials. Typical examples are blast-furnace slags,[39,44] fly and bottom ash,[38,40,41,43,45,46] newsprint recycling residues,[34,47,48] soda-lime-silica glass,[49] carbonated opoka,[50] oil shale ash,[51] and cement bypass dust.[52]

Based on these literature data and considering the need to find additional reuse strategies for KRY·AS and DGC, we report here a method to synthesize a tobermorite-rich material (TRM) from a proper mixture of KRY·AS and a fine (0−50 μm) glass powder derived from DGC processing. The TRM, after characterization, has been tested as a selective adsorbent for toxic metals in multielement aqueous solutions.

2. MATERIALS AND METHODS

2.1. Source Materials. The chemical composition of KRY·AS and the glass powder is listed in Table 1. The same materials were already described and employed in past research activities,[53] and they are mainly composed of calcium carbonate and calcium silicates (KRY·AS) and by amorphous materials with a small amount of crystalline calcium carbonate and metal aluminum (glass powder).

As mentioned, KRY·AS is the product of the thermal inertization of CAS performed in industrial kilns at temperatures in the range of 1200−1300 °C.[7] The obtained product is free of asbestos phases and contains newly formed clinker

https://doi.org/10.1021/acsomega.1c04193
ACS Omega 2022, 7, 1694−1702

phases with cytotoxic effects comparable to those of commercial clinker.[9] More specifically, KRY·AS is composed of subspherical particles of the newly formed crystalline phases but with an excess of aluminum, iron, and magnesium and a compositional variability mostly depending on the provenience of the CAS.[10] Glass powder is from the sleeve filters of the mills used to grind glass from domestic recycling. It should be emphasized that due to the small grain size (less than 50 μm) and the occurrence of a small amount of Mg and Fe, the recovery options are quite limited, and this powder is generally considered a waste.

2.2. Synthesis Procedure. Al-substituted tobermorites can be successfully obtained in a simulated hydrothermal environment from materials whose composition approximately falls within the molar ratios $0.80 < Ca/[Si + Al + Fe] < 0.85$ and $0.00 < [Al + Fe]/[Al + Si + Fe] < 0.17$.[31,48,52] Even if various approaches have been attempted in the past to optimize the reaction mechanism mainly by varying the reaction time, temperature, and reagents (see the literature cited in the Introduction), to date, the synthesis of a pure form of tobermorite has not yet been obtained. The optimization of the synthesis parameters to gain the maximum amount of tobermorite in the final product goes beyond the aim of this research as our primary goal is maximizing the quantity of waste recovery as opposed to lower energy consumption. The hydrothermal synthesis was carried out in a Teflon-lined Parr bomb by adding 15 mL of NaOH 1 M solution to 1 g of a mixture (KGT, Table 1) prepared by dosing KRY·AS (66.5 wt %), glass powder (31.5 wt %), and a small amount (2.0 wt %) of a phillipsite-rich zeolitic tuff to fix the molar ratios defined above. The phillipsite-rich zeolitic tuff was introduced as phillipsite was found to be a catalyst for the synthesis of tobermorite;[54] besides, it has very limited costs and can also be found as quarry production waste.[55] The bomb was disposed in a kiln at 120 °C for 24 h on a basculation plan (60 oscillations per min) to favor the interaction between the powder and the solution. After cooling, the solid (i.e., TRM) was separated from residual solution, washed with distilled water until the pH of the washing water was about neutral (about 7.1), dried at 50 °C overnight, gently disaggregated in an agate mortar, passed through a 100 μm sieve, and then characterized and used in the adsorption experiments.

2.3. Adsorption Kinetics and Removal Selectivity of Toxic Metals from Aqueous Solutions. The adsorption kinetics of Ni^{2+}, Zn^{2+}, Cd^{2+}, and Pb^{2+} were measured from multielement solutions prepared with reagent-grade salts (acetates) from Sigma-Aldrich. The concentrations tested were 100, 50, 10, 5, and 1 mmol/L; in the solutions, the molar content of each cation was the same to neutralize preferential adsorption due to difference in ionic strength (all the considered cations being divalent and also the charge-equivalent concentration is identical). More specifically, this range of concentrations was chosen to fit, as best as possible, with those already studied in the past in similar research studies.[33−36,56,57] Adsorption experiments were carried out preparing single batch suspensions with 100 mg of the TRM and 30 mL of solution;[34] this ratio ensures, even at the lowest concentration, a quantity of cations in solution that can saturate the adsorbing capacity of the TRM. The batches were shaken at 250 rpm in an orbital incubator (Stuard Scientific Orbital Incubator SI50) at 20 °C (Haake k20 thermocryostat) for 1, 2, 4, 8, 16, 32, 64, and 128 h which, based on literature data,[34,39] should be sufficient time to reach equilibrium. Afterward, the supernatant liquors were recovered by centrifugation at 8000 rpm (Thermo mod. Espresso) for 5 min, acidified with 0.1 mL of HNO_3 to prevent salt precipitation, and analyzed. The pH of each batch solution was checked before and after the adsorption experiments.

2.4. Analytical Methods. We applied a consolidated analytical protocol for materials characterization encompassing X-ray powder diffraction (XRPD) measurements with the Rietveld method for the quantitative phase analyses (QPAs), thermogravimetric analyses coupled with evolved gas detection through mass spectrometry (TGA−MSEGA), chemical analyses by X-ray fluorescence, elemental analyses (EA), and inductively coupled plasma optical emission spectroscopy.[7,53,58−62] Further details about preliminary sample preparation, methods, instruments, experimental conditions, and data analyses are provided in the Supporting Information.

3. RESULTS

The chemical analyses (Table 1) showed that part of Na provided through the alkaline solution moved from a liquid to a solid phase as its concentration increases in the TRM with respect to KGT. On the contrary, the concentration of the other elements, likely involved in the chemical substitutions in tobermorite, has not changed significantly, suggesting that they contributed almost completely to the formation of crystalline phases or precipitated as amorphous materials rather than remaining in the solution and being removed when the solid is separated from the liquid after the synthesis.

The XRPD measurements of the TRM (Figure 1) showed the occurrence of 11 Å-tobermorite, aragonite, and calcite. The

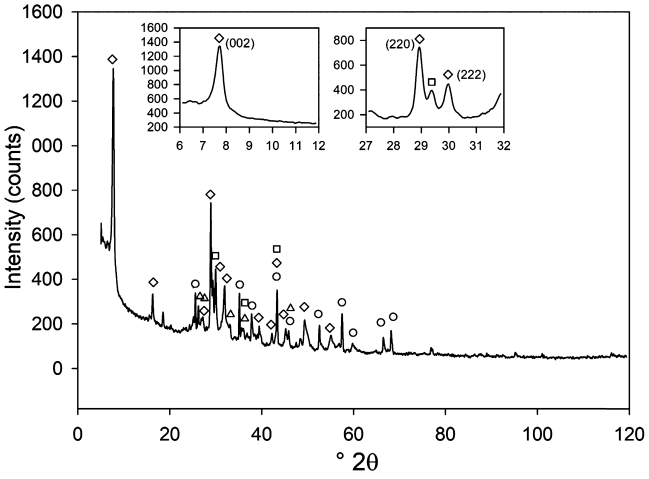

Figure 1. XRPD pattern of the TRM with corundum as an internal standard. Symbols denote the main reflection planes of tobermorite (diamond), aragonite (triangle), calcite (square), and corundum (circle). In the two magnifications are shown zoomed views of the 6−12 and 27−32° 2θ ranges.

basal spacing defined by the (002) reflection plane in tobermorite is 11.43 Å, thus in good agreement with values previously reported for Al-substituted tobermorites.[39,48] There is no evidence of the occurrence of 9 Å- and 14 Å-tobermorites as the main reflections are lacking and/or mismatched. The model from Mitsuda and Taylor (1975) was applied to estimate the crystallinity rate of the synthesized tobermorite.[63] This model defines four levels of crystallinity in Al-substituted tobermorites based on the occurrence and shape of the (002),

https://doi.org/10.1021/acsomega.1c04193
ACS Omega 2022, 7, 1694−1702

(220), and (222) reflection planes which are as follows: Level A, (002) absent; Level B, broad (002), unresolved (220) and (222); Level C, occurrence of (002), partial resolution of (220) and (222); and Level D, sharp basal reflection and clearly resolved (220) and (222). In the XRPD pattern of the TRM (Figure 1), the three reflections are well evident and sharp, thus suggesting a high grade of crystallinity (Level D).

The QPA of the TRM was carried out applying the Rietveld method and using as starting structural models for the refinement those from Yamazaki and Toraya (2001) for Al-substituted 11 Å-tobermorite (COD code 1527001),[64] Villiers (1971) for aragonite (COD code 5000085),[65] and Sitepu (2009) for calcite (COD code 9016022).[66] The QPA results (Table 2 and Figure S2) better detailed the occurrence of a large amount of 11 Å-tobermorite and a lesser content of aragonite and calcite. Moreover, the addition of a standard to the raw sample powder to apply a combination of the Rietveld and the RIR methods highlighted the significant presence of an amorphous phase. The refinement carried out using the structure of a tobermorite without substitutions produced a worse agreement.

Table 2. Quantitative Phase Analyses of the TRM[a]

	weight %
11 Å-tobermorite	53.4(6)
aragonite	7.6(2)
calcite	2.3(1)
amorphous	36.7(7)
$\chi 2$	0.7833
R_p	0.0562
R_{wp}	0.0785

[a]The standard deviation σ_Q (values in parenthesis) of the weight percentage Q of each phase was calculated through the GSAS software and applying the formula $\sigma_Q = \{[(\sigma_a/a)^2 + (\sigma_b/b)^2]^{1/2}\} Q$, where a and b are the two variables most affecting Q values and refer to the weight fraction of the phase and the internal standard, respectively, whereas σ_a and σ_b are their standard deviations.[58]

The TGA and its first derivative (DTG) curves (Figure 2a) showed three main thermal events as follows: (1) 25−310 °C (maximum reaction rate at 133 °C; mass loss 10.11 wt %), (2) 315−410 °C (362 °C; 2.03 wt %), and (3) 495−740 °C (676 °C; 5.36 wt %). An additional minor high-temperature reaction (4) also occurs between 750 and 865 °C with the maximum rate at 805 °C and a weight loss of 0.27 wt %. The reaction (1) is related to the removal of zeolitic water (m/z = 18, Figure 2b) in tobermorite. The reaction (2) is due to the thermal decomposition of (amorphous) hydroxides as shown by the release of water (m/z = 18); it is out of the aim of this work to characterize these compounds, but it is reasonable that they should have a brucite-like structure as Mg, present in KGT (Table 1), is hardly incorporated into the tobermorite framework. The reaction (3), which is the sum of at least two different thermal events as indicated by the shoulder on the DTG curve at about 600 °C, is due to decarbonation of aragonite (shoulder) and calcite, as demonstrated by the release of CO_2 (m/z = 44, Figure 2a). The interpretation of the reaction (4) is trickier as it involves a very low amount of the material, and the released gases were not identified.

The total amount of carbonates can be calculated from the mass loss due to decarbonation (Reaction 3, Figure 2a), and the result (12.2 wt %) is in good agreement with the Rietveld refinement data (9.9 wt %, sum of aragonite and calcite, Table 2). Likewise, the moles of Ca hosted in the two carbonates (0.09891 and 0.1219 mol/100 g from QPA and TGA, respectively) can be calculated from the mineral formula. Reactions that involve the release of NO (m/z = 30) and SO_2 (m/z = 64) were not observed, and the absence of nitrogen and sulfur was confirmed through EA.

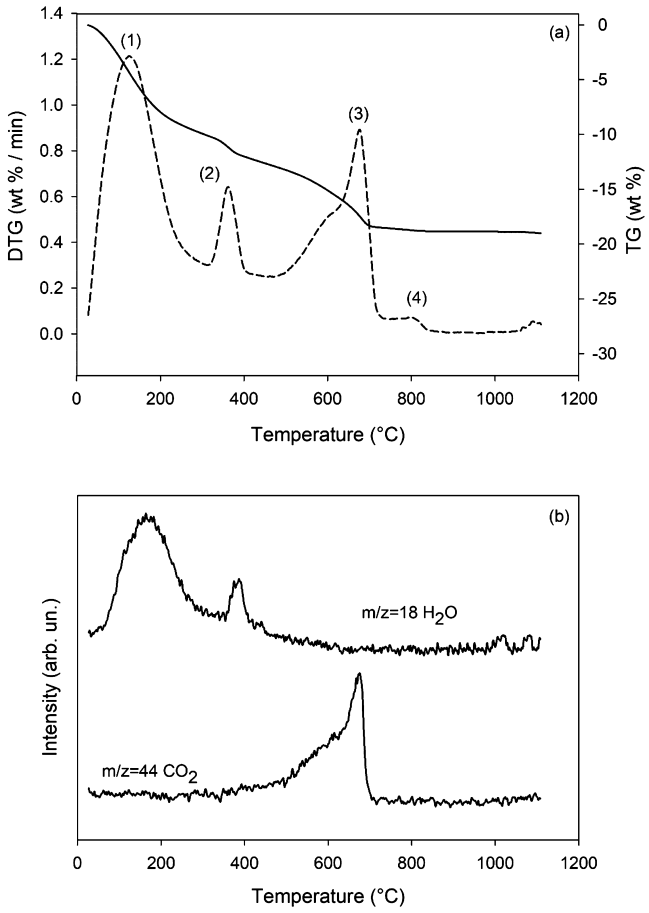

Figure 2. Thermal behaviour of the TRM. (a) TG (solid black line) and DTG (dashed black line). (b) MSEGA curves. Numbers on the DTG curve refer to thermal reactions described in the text.

The time-dependent removal of metal cations (Figures 3 and S3) was evaluated considering the dependence between the concentration of the elements in solution at room temperature and the unit mass of the adsorbent (TRM). The results shown in Figure 3 clearly indicated that cations are selectively removed and the higher the concentration of metals in solution, the greater the selectivity (Figure 3a−c). Pb^{2+} is the cation that is preferentially removed followed, in order, by Zn^{2+}, Cd^{2+}, and Ni^{2+}. The removal of Cd^{2+} is comparable to that of Ni^{2+} only in the batches prepared with the solutions at concentrations 1 and 5 mmol/L (Figure 3d,e, respectively) while that of Zn^{2+} and, mostly, of Pb^{2+} remains high and selective. The kinetic curves shown in Figure 3 also showed that the removal takes place fairly and quickly and the equilibrium is almost reached in the first 8 h (only in the 100 and 50 mmol/L batches, the saturation is reached just faster than in the others). The representation by the weight % of the total amount of toxic metals removed by the TRM may be relevant for applicative purposes and is shown in Figure 3f. This analysis highlights how the overall adsorption depends on

https://doi.org/10.1021/acsomega.1c04193
ACS Omega 2022, 7, 1694−1702

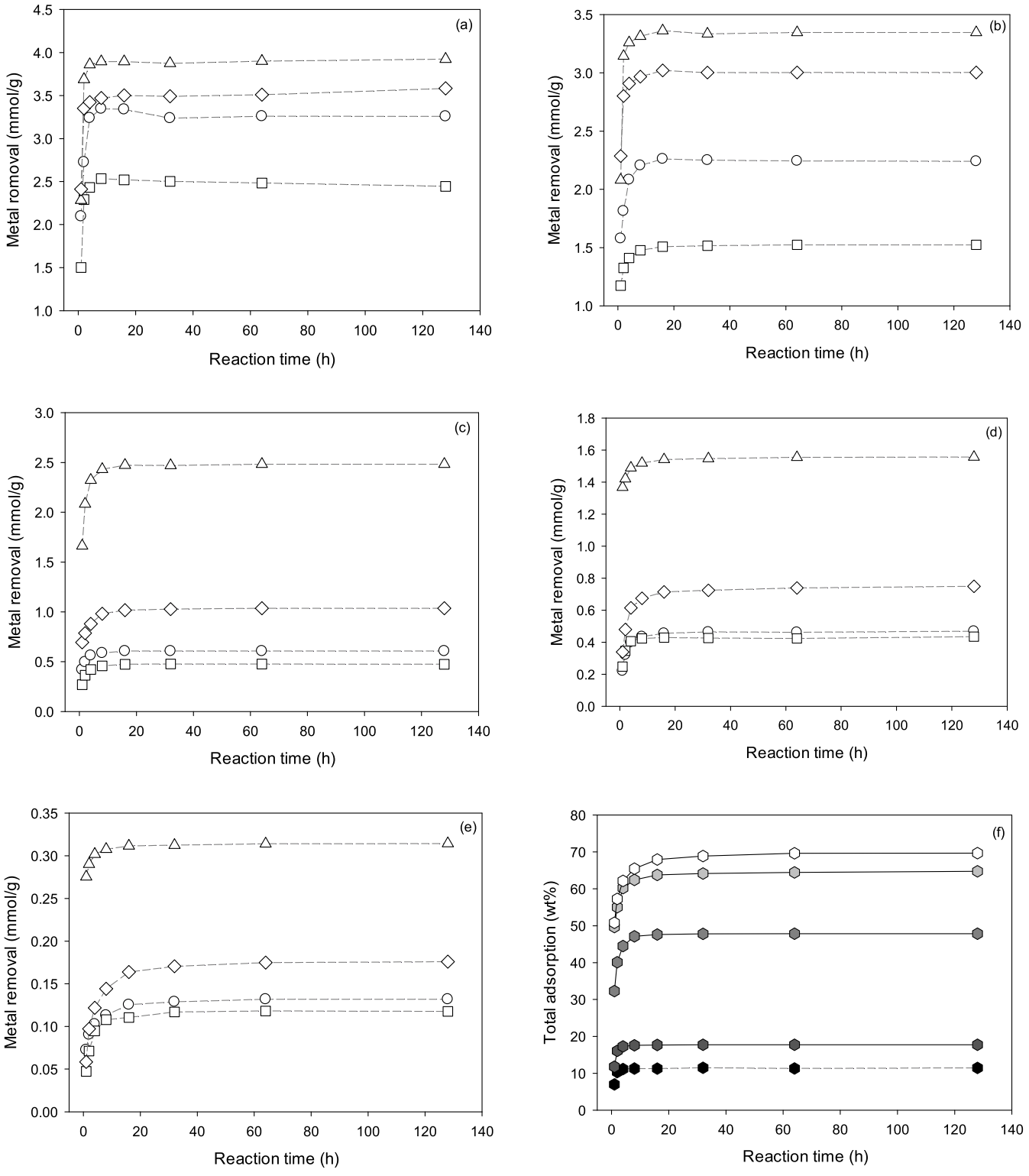

Figure 3. Time-dependent metal cation removal from 100 (a), 50 (b), 10 (c), 5 (d), and 1 (e) mmol/L aqueous solutions. Triangle, Pb^{2+}; diamond, Zn^{2+}; circle, Cd^{2+}; and square, Ni^{2+}. (f) Total amount of metal cations removed. The gray scale of the symbols in f indicates the concentrations of the solutions from 100 (black) to 1 mmol/L (white).

the concentration of the solution, and it varies between 10 and 70 wt % for the highest (100 mmol/L) and lowest (1 mmol/L) concentrations, respectively. An analogue representation for each batch is shown in Figure S3.

4. DISCUSSION

The experimental results presented in this work clearly indicate that it is possible to synthesize tobermorite using end-of-waste materials. The whole compositional range for 11 Å-tobermorite, without accounting Al^{3+} and Fe^{3+} for Si^{4+} substitutions, spans between $Ca_4Si_6O_{15}(OH)_2{\cdot}5H_2O$ when

https://doi.org/10.1021/acsomega.1c04193
ACS Omega 2022, 7, 1694−1702

no zeolitic Ca occupies the interlayer and $Ca_5Si_6O_{17}\cdot 5H_2O$ when one Ca cation per unit formula is hosted in the interlayer space.[67] Based on the goodness of fit of the Rietveld refinement (Table 2 and Figure S2) achieved using an Al-substituted tobermorite as the starting model,[64] it can be argued that in TRM tobermorite, Si^{4+} is partly substituted by Al^{3+} and, likely, by Fe^{3+}. This conclusion is in agreement with the chemical data as in the TRM, the [Al + Fe]/[Si + Al + Fe] molar ratio of 0.125 is in the optimal range of 0.00−0.17, typical of substituted tobermorite, as well as the [Al]/[Al + Si] molar ratio of 0.097 is below the maximum value of 0.13−0.14.[31,48,52,68] In TRM tobermorite, Al^{3+} and Fe^{3+} for Si^{4+} substitutions are balanced by the occurrence in the interlayer of Ca^{2+} and, likely, Na^+ and K^+ cations rather than by $(OH)^-$ for O^{2-} substitutions, as suggested by the absence of thermal events related to a dehydroxylation reaction which should occur between 550 and 650 °C.[69] The contribution of Na^+ and K^+ to the charge balance is necessary as a nonnegligible amount of Ca (0.1104 mol/100 g, calculated averaging the concentration values from QPA and TGA) is hosted in the calcite and aragonite lattice. Therefore, the charge deficit provided by Al^{3+} and Fe^{3+} for Si^{4+} substitutions (0.3030 equiv/100 g, Table S1) cannot be neutralized only by exchangeable Ca^{2+} in tobermorite (ideally 1/5, thus 0.2209 equiv/100 g in TRM tobermorite). Nevertheless, these considerations are based on the constraint that in the amorphous phase there are no compounds with a tobermorite-like structure.

The crystallization of carbonates, as well as that of other compounds such as C−S−H phases (the latter being not found in the TRM), could sound unusual; nevertheless, it has already been observed in other similar synthesis experiments.[52,70−73] More specifically, the crystallization of calcite and aragonite is due to progressive and time-dependent carbonation reactions and here, it could be favored by the occurrence of calcite in the source materials which could have acted as a catalyst.[70] The high amount of the amorphous phase is reasonably due to the short times used for the synthesis (although, as mentioned, the synthesis of a pure form of tobermorite has never been reported in the literature to date) and to the presence in the source materials (mostly in KRY·AS) of huge amounts of Mg that can hardly be incorporated into the structure of tobermorite. In contrast, the short time of synthesis does not affect the crystallinity of the tobermorite phase.

The adsorption curves (Figure 3) showed that the TRM, like other synthetic materials with similar mineralogical composition, may remove toxic metals from aqueous solutions. Nevertheless, metal removal must occur not only by cation-exchange reactions but also by surface adsorption. In fact, with the exception of the 1 mmol/L batch, the charge equivalents of metal cations removed are higher than those related to exchangeable Ca^{2+}, Na^+, and K^+ in the TRM (Table S2). Therefore, inner- and outer-sphere bonding may occur either with the exposed oxygens of tobermorite and the hydroxyls forming the amorphous phase.[74,75] This hypothesis is confirmed by considering the small increase (between 0.1 and 0.3) of pH observed at the end of each treatment and attributed to zeolitic Ca^{2+}, Na^+, and K^+ cations released by tobermorite (metal cations, in view of the partial deprotonation of their aqua complexes, are more acidic). The adsorption rate of the 100 and 50 mmol/L solutions is very close (only a little faster) to that observed for the other concentrations. Although there is no direct experimental evidence, it is possible that this atypical behavior is due to the occurrence of unsaturated negative charges (e.g., those related to amorphous materials) which affects the adsorption process. Regardless of all the considered metals being divalent, the cation-exchange reactions should first involve the release of Na^+ which has less affinity for the tobermorite interlayer.[39,76]

The high affinity of 11 Å-tobermorite toward toxic metals had been observed before,[34,35,39,43] but the competitive adsorption from multielement solution had rarely been verified.[39] In the case of the TRM, it should be stressed that the markedly selective removal of metal cations is not opposed by fluctuating time-dependent adsorption paths. Indeed, with the exception of a slight decrease in the removal rate of Cd^{2+} and Ni^{2+} between 16 and 32 h in the 100 mmol/L batch, the equilibrium conditions, once reached, are preserved over a time span of almost 100 h. This behavior distinguishes the TRM from other materials such as zeolitized tuffs and clay minerals where consecutive adsorption/desorption reactions may occur over time.[77−79]

In recent years, waste recovery and exploitation have become options playing a strategic role in drastically reducing final disposal in landfills while ensuring increasing quantities of secondary raw materials. Currently, the main interest for tobermorite is due to its occurrence in cements as it improves thermal and acoustic insulating properties. On the other hand, the use of tobermorite as an adsorbent does not yet have a significant impact in large-scale applications, probably due to the availability of NRM (mainly bentonites and zeolitic tuffs) with similar, or even better, adsorption performance. However, it should be emphasized that tobermorite-rich materials (like the TRM but also others mentioned in the Introduction) have a CEC close to that of natural bentonites (i.e., ranging approximately between 60 and 120 meq/100 g) and just below that of several zeolitic tuffs (i.e., 100−200 meq/100 g).[80−82] Even without a detailed market analysis, it is reasonable to assume that the large-scale production of tobermorite using only pure reagents would be impractical as it would cost significantly more than the mining and trade of NRM. Nevertheless, it is also true that the use of NRM has a high impact on the environment (opening/expanding of quarries is always a hotly debated issue), especially if this is countered by a possible green solution to gain materials with similar properties. In addition, it is also conceivable that the environmental benefits of replacing NRM with waste-derived materials outweigh the overall impact of the collection, sorting, transport, and recycling of waste, and the cost of these operations can be recovered by the sale of the synthesized materials.

5. CONCLUSIONS

The main objective of this work was to test KRY·AS and DGC as possible candidates for a fast and environmentally friendly synthesis of a microporous material to be used for the removal of toxic metals from aqueous solutions. Although the tests were carried out at the laboratory scale, we believe that the transfer to a larger scale should not meet major impediments, either in relation to the simple preparatory procedure and the mild conditions under which the synthesis is carried out.

Despite the relevant properties of the TRM, we are aware that the method described here addresses two obstacles that may slow down its large-scale application: (i) the chemical composition of the waste which may vary depending on the source and (ii) the occurrence of NRM with similar properties

https://doi.org/10.1021/acsomega.1c04193
ACS Omega 2022, 7, 1694−1702

available at lower costs. The former, however, is of little impact as it is sufficient to calculate the amount of each waste to meet the synthesis protocol. On the other hand, the availability of analogue NRM (e.g., bentonites and zeolitic tuffs) is a more sensitive issue and, to be critically commented, would require a thorough analysis of the cost-benefit ratio, also properly assessing the overall environmental impact.

■ ASSOCIATED CONTENT

Supporting Information

The Supporting Information is available free of charge at https://pubs.acs.org/doi/10.1021/acsomega.1c04193.

Details about analytical methods and sample preparation before measurements, instruments, experimental conditions and data analyses; sketch of the tobermorite structure; graphical results of the Rietveld refinement of the TRM; time-dependent metal cation removal in weight %; and chemical analyses of the TRM considering the repartition of Ca between tobermorite and the sum of calcite and aragonite (PDF)

■ AUTHOR INFORMATION

Corresponding Author

Daniele Malferrari − *Department of Chemical and Geological Sciences, The University of Modena and Reggio Emilia, Modena I-41125, Italy;* orcid.org/0000-0002-0879-1703; Email: daniele.malferrari@unimore.it

Authors

Fabrizio Bernini − *Department of Chemical and Geological Sciences, The University of Modena and Reggio Emilia, Modena I-41125, Italy;* orcid.org/0000-0002-2598-7716

Dario Di Giuseppe − *Department of Chemical and Geological Sciences, The University of Modena and Reggio Emilia, Modena I-41125, Italy*

Valentina Scognamiglio − *Department of Chemical and Geological Sciences, The University of Modena and Reggio Emilia, Modena I-41125, Italy*

Alessandro F. Gualtieri − *Department of Chemical and Geological Sciences, The University of Modena and Reggio Emilia, Modena I-41125, Italy;* orcid.org/0000-0002-4414-9603

Complete contact information is available at: https://pubs.acs.org/10.1021/acsomega.1c04193

Notes

The authors declare no competing financial interest.

■ ACKNOWLEDGMENTS

We warmly acknowledge the competent reviewers for their advices to improve our manuscript and the editor for the quick and accurate management of the review process. This research is under the contribution of the grants: (1) "Mineral Reactivity, a Key to Understand Large-Scale Processes: from Rock Forming Environments to Solid Waste Recovering/Lithification" (grant code PRIN2017L83S77) and (2) "Fibres, A Multidisciplinary Mineralogical, Crystal-Chemical and Biological Project to Amend the Paradigm of Toxicity and Cancerogenicity of Mineral Fibres" (grant code PRIN20173X8WA4). We also thank ZETADI srl. for providing the KRY·AS end-of-waste. This work does not require any institution and ethics approval, neither informed consent, and the authors declare no conflicts of interest.

■ REFERENCES

(1) Schoer, K.; Weinzettel, J.; Kovanda, J.; Giegrich, J.; Lauwigi, C. Raw Material Consumption of the European Union − Concept, Calculation Method, and Results. *Environ. Sci. Technol.* **2012**, *46*, 8903−8909.

(2) Bauwens, T.; Hekkert, M.; Kirchherr, J. Circular Futures: What Will They Look Like? *Ecol. Econ.* **2020**, *175*, 106703.

(3) Getor, R. Y.; Mishra, N.; Ramudhin, A. The Role of Technological Innovation in Plastic Production within a Circular Economy Framework. *Resour. Conserv. Recycl.* **2020**, *163*, 105094.

(4) Greer, R.; von Wirth, T.; Loorbach, D. The Diffusion of Circular Services: Transforming the Dutch Catering Sector. *J. Clean. Prod.* **2020**, *267*, 121906.

(5) Steenmans, K.; Malcolm, R. Transitioning towards Circular Systems: Property Rights in Waste. *J. Prop. Plan. Environ. Law* **2020**, *12*, 219−234.

(6) IBAS. Current Asbestos Bans. http://www.ibasecretariat.org/alpha_ban_list.php (accessed Aug 03, 2021).

(7) Gualtieri, A. F.; Cavenati, C.; Zanatto, I.; Meloni, M.; Elmi, G.; Gualtieri, M. L. The Transformation Sequence of Cement−Asbestos Slates up to 1200°C and Safe Recycling of the Reaction Product in Stoneware Tile Mixtures. *J. Hazard. Mater.* **2008**, *152*, 563−570.

(8) Gualtieri, A. F.; Gualtieri, M. L.; Tonelli, M. In Situ ESEM Study of the Thermal Decomposition of Chrysotile Asbestos in View of Safe Recycling of the Transformation Product. *J. Hazard. Mater.* **2008**, *156*, 260−266.

(9) Pugnaloni, A.; Lucarini, G.; Rubini, C.; Smorlesi, A.; Tomasetti, M.; Strafella, E.; Armeni, T.; Gualtieri, A. F. Raw and Thermally Treated Cement Asbestos Exerts Different Cytotoxicity Effects on A549 Cells in Vitro. *Acta Histochem.* **2015**, *117*, 29−39.

(10) Viani, A.; Gualtieri, A. F.; Pollastri, S.; Rinaudo, C.; Croce, A.; Urso, G. Crystal Chemistry of the High Temperature Product of Transformation of Cement-Asbestos. *J. Hazard. Mater.* **2013**, *248-249*, 69−80.

(11) Viani, A.; Gualtieri, A. F.; Secco, M.; Peruzzo, L.; Artioli, G.; Cruciani, G. Minerals in the Human. Body Crystal Chemistry of Cement-Asbestos. *Am. Mineral.* **2013**, *98*, 1095−1105.

(12) US EPA, O. Glass: Material-Specific Data. https://www.epa.gov/facts-and-figures-about-materials-waste-and-recycling/glass-material-specific-data (accessed Sept 08, 2021).

(13) Honma, S.; Hu, J.-L. Cost Efficiency of Recycling and Waste Disposal in Japan. *J. Clean. Prod.* **2021**, *284*, 125274.

(14) TGM. Eurostat. https://ec.europa.eu/eurostat/web/main/help/first-visit/tgm (accessed Sept 08, 2021).

(15) Testa, M.; Malandrino, O.; Sessa, M. R.; Supino, S.; Sica, D. Long-Term Sustainability from the Perspective of Cullet Recycling in the Container Glass Industry: Evidence from Italy. *Sustainability* **2017**, *9*, 1752.

(16) Jiang, Y.; Ling, T.-C.; Mo, K. H.; Shi, C. A Critical Review of Waste Glass Powder − Multiple Roles of Utilization in Cement-Based Materials and Construction Products. *J. Environ. Manage.* **2019**, *242*, 440−449.

(17) Lebullenger, R.; Mear, F. O. *Glass Recycling*; Springer Handb, 2019; pp 1355−1377.

(18) Elmes, V. K.; Edgar, B. N.; Mendham, A. P.; Coleman, N. J. Basic Metallosilicate Catalysts from Waste Green Container Glass. *Ceram. Int.* **2018**, *44*, 17069−17073.

(19) Guadagnino, E.; Gambaro, M.; Gramiccioni, L.; Denaro, M.; Feliciani, R.; Baldini, M.; Stacchini, P.; Giovannangeli, S.; Carelli, G.; Castellino, N.; Vinci, F. Estimation of Lead Intake from Crystalware under Conditions of Consumer Use. *Food Addit. Contam.* **2000**, *17*, 205−218.

(20) Bessmertniy, V. S.; Klimenko, V. A.; Bondarenko, M. A.; Olisov, A. V.; Bragina, L. L. Glass Micro Balls Based on Glass Domestic Waste for Road Construction. *Mater. Sci. Forum* **2021**, *1017*, 111−121.

(21) Mutafela, R. N.; Ye, F.; Jani, Y.; Dutta, J.; Hogland, W. Efficient and Low-Energy Mechanochemical Extraction of Lead from Dumped Crystal Glass Waste. *Environ. Chem. Lett.* **2021**, *19*, 1879−1885.
(22) Jamshidi, A.; Kurumisawa, K.; Nawa, T.; Igarashi, T. Performance of Pavements Incorporating Waste Glass: The Current State of the Art. *Renew. Sustain. Energy Rev.* **2016**, *64*, 211−236.
(23) Silva, R. V.; de Brito, J.; Lye, C. Q.; Dhir, R. K. The Role of Glass Waste in the Production of Ceramic-Based Products and Other Applications: A Review. *J. Clean. Prod.* **2017**, *167*, 346−364.
(24) Luhar, S.; Luhar, I. Potential Application of E-Wastes in Construction Industry: A Review. *Constr. Build. Mater.* **2019**, *203*, 222−240.
(25) Khan, M. N. N.; Saha, A. K.; Sarker, P. K. Reuse of Waste Glass as a Supplementary Binder and Aggregate for Sustainable Cement-Based Construction Materials: A Review. *J. Build. Eng.* **2020**, *28*, 101052.
(26) Adekomaya, O.; Majozi, T. Mitigating Environmental Impact of Waste Glass Materials: Review of the Existing Reclamation Options and Future Outlook. *Environ. Sci. Pollut. Res.* **2021**, *28*, 10488−10502.
(27) Merlino, S.; Bonaccorsi, E.; Armbruster, T. The Real Structure of Tobermorite 11A: Normal and Anomalous Forms, OD Character and Polytypic Modifications. *Eur. J. Mineral.* **2001**, *13*, 577−590.
(28) Bonaccorsi, E.; Merlino, S. Modular Microporous Minerals: Cancrinite-Davyne Group and C-S-H Phases. *Rev. Mineral. Geochem.* **2005**, *57*, 241−290.
(29) Biagioni, C.; Merlino, S.; Bonaccorsi, E. The Tobermorite Supergroup: A New Nomenclature. *Mineral. Mag.* **2015**, *79*, 485−495.
(30) McConnell, J. D. C. The Hydrated Calcium Silicates Riversideite, Tobermorite, and Plombierite. *Mineral. Mag. J. Mineral Soc.* **1954**, *30*, 293−305.
(31) Diamond, S.; White, J. L.; Dolch, W. L. Effects of Isomorphous Substitution in Hydrothermally-Synthesized Tobermorite. *Am. Mineral.* **1966**, *51*, 388−401.
(32) Suhasini, R. Autoclaving Cement Concrete: A Review. *Int. J. Appl. Eng. Res.* **2014**, *9*, 1603−1617.
(33) Komarneni, S. Heavy Metal Removal from Aqueous Solutions by Tobermorites and Zeolites. *Nucl. Chem. Waste Manag.* **1985**, *5*, 247−250.
(34) Coleman, N. J. Interactions of Cd(II) with Waste-Derived 11 Å Tobermorites. *Sep. Purif. Technol.* **2006**, *48*, 62−70.
(35) Coleman, N. J.; Brassington, D. S.; Raza, A.; Mendham, A. P. Sorption of Co2+ and Sr2+ by Waste-Derived 11 Å Tobermorite. *Waste Manag.* **2006**, *26*, 260−267.
(36) Coleman, N. J.; Brassington, D. S.; Raza, A.; Lee, W. E. Calcium Silicate Sorbent from Secondary Waste Ash: Heavy Metals-Removal from Acidic Solutions. *Environ. Technol.* **2006**, *27*, 1089−1099.
(37) Qi, H. B.; Du, H.; Yin, C. C. Experimental Research on Adsorption of Cadmium with Synthetic Tobermorite from Wastewater. *Adv. Mater. Res.* **2011**, *160*−*162*, 1038−1043.
(38) Chiang, Y. W.; Ghyselbrecht, K.; Santos, R. M.; Meesschaert, B.; Martens, J. A. Synthesis of Zeolitic-Type Adsorbent Material from Municipal Solid Waste Incinerator Bottom Ash and Its Application in Heavy Metal Adsorption. *Catal. Today* **2012**, *190*, 23−30.
(39) Tsutsumi, T.; Nishimoto, S.; Kameshima, Y.; Miyake, M. Hydrothermal Preparation of Tobermorite from Blast Furnace Slag for Cs+ and Sr2+ Sorption. *J. Hazard. Mater.* **2014**, *266*, 174−181.
(40) Wajima, T. Synthesis of Tobermorite from the Ash after Treatment of Asbesto-Containing Disaster Waste, and Its Removal Ability of Cs(I) from Aqueous Solution. *Eng. J.* **2016**, *20*, 79−91.
(41) Zou, J.; Guo, C.; Zhou, X.; Sun, Y.; Yang, Z. Sorption Capacity and Mechanism of Cr3+ on Tobermorite Derived from Fly Ash Acid Residue and Carbide Slag. *Colloids Surf., A* **2018**, *538*, 825−833.
(42) Baldermann, A.; Landler, A.; Mittermayr, F.; Letofsky-Papst, I.; Steindl, F.; Galan, I.; Dietzel, M. Removal of Heavy Metals (Co, Cr, and Zn) during Calcium−Aluminium−Silicate−Hydrate and Trioctahedral Smectite Formation. *J. Mater. Sci.* **2019**, *54*. https://doi.org/ DOI: 10.1007/s10853-019-03541-5.
(43) Guo, X.; Li, D. Solidification/Adsorption of Heavy Metals by FA/FA-MSWI Based Al-Substituted Tobermorite. *J. Wuhan Univ. Technol., Mater. Sci. Ed.* **2019**, *34*, 1345−1349.
(44) Jing, Z.; Jin, F.; Hashida, T.; Yamasaki, N.; Ishida, H. Hydrothermal Solidification of Blast Furnace Slag by Formation of Tobermorite. *J. Mater. Sci.* **2007**, *42*, 8236−8241.
(45) Ma, W.; Brown, P. W. Hydrothermal Synthesis of Tobermorite from Fly Ashes. *Adv. Cem. Res.* **1997**, *9*, 9−16.
(46) Ding, J.; Tang, Z.; Ma, S.; Wang, Y.; Zheng, S.; Zhang, Y.; Shen, S.; Xie, Z. A Novel Process for Synthesis of Tobermorite Fiber from High-Alumina Fly Ash. *Cem. Concr. Compos.* **2016**, *65*, 11−18.
(47) Coleman, N. J.; Brassington, D. S. Synthesis of Al-Substituted 11 Å Tobermorite from Newsprint Recycling Residue: A Feasibility Study. *Mater. Res. Bull.* **2003**, *38*, 485−497.
(48) Coleman, N. J. Synthesis, Structure and Ion Exchange Properties of 11Å Tobermorites from Newsprint Recycling Residue. *Mater. Res. Bull.* **2005**, *40*, 2000−2013.
(49) Lamidi, Y. D.; Owoeye, S. S.; Abegunde, S. M. Preparation and Characterization of Synthetic Tobermorite (CaO−Al2O3−SiO2−H2O) Using Bio and Municipal Solid Wastes as Precursors by Solid State Reaction. *Bol. Soc. Esp. Ceram.* **2020**, DOI: 10.1016/j.bsecv.2020.07.003.
(50) Smalakys, G.; Siauciunas, R. The Synthesis of 1.13 Nm Tobermorite from Carbonated Opoka. *J. Therm. Anal. Calorim.* **2018**, *134*, 493−502.
(51) Reinik, J.; Heinmaa, I.; Mikkola, J.-P.; Kirso, U. Hydrothermal Alkaline Treatment of Oil Shale Ash for Synthesis of Tobermorites. *Fuel* **2007**, *86*, 669−676.
(52) Coleman, N. J.; Trice, C. J.; Nicholson, J. W. 11 Å Tobermorite from Cement Bypass Dust and Waste Container Glass: A Feasibility Study. *Int. J. Miner. Process.* **2009**, *93*, 73−78.
(53) Ligabue, M. L.; Gualtieri, A. F.; Gualtieri, M. L.; Malferrari, D.; Lusvardi, G. Recycling of Thermally Treated Cement-Asbestos for the Production of Porcelain Stoneware Slabs. *J. Clean. Prod.* **2020**, *247*, 119084.
(54) Komarneni, S.; Komarneni, J. S.; Newalkar, B.; Stout, S. Microwave-Hydrothermal Synthesis of Al-Substituted Tobermorite from Zeolites. *Mater. Res. Bull.* **2002**, *37*, 1025−1032.
(55) Faccini, B.; Di Giuseppe, D.; Malferrari, D.; Coltorti, M.; Abbondanzi, F.; Campisi, T.; Laurora, A.; Passaglia, E. Ammonium-Exchanged Zeolitite Preparation for Agricultural Uses: From Laboratory Tests to Large-Scale Application in ZeoLIFE Project Prototype. *Period. Mineral.* **2015**, *84*, 303−321.
(56) Komarneri, S.; Roy, D. M.; Roy, R. Al-Substituted Tobermorite: Shows Cation Exchange. *Cem. Concr. Res.* **1982**, *12*, 773−780.
(57) Miyake, M.; Komarneni, S.; Roy, R. Kinetics, Equilibria and Thermodynamics of Ion Exchange in Substituted Tobermorites. *Mater. Res. Bull.* **1989**, *24*, 311−320.
(58) Young, H. D. *Statistical Treatment of Experimental Data*; McGraw-Hill Book Company: New York, 1962.
(59) Larson, A. C.; Von Dreele, R. B. *General Structure Analysis System (GSAS) Report LAUR 86-748*; Los Alamos National Laboratory, 1994.
(60) Toby, B. H. EXPGUI, a Graphical User Interface for GSAS. *J. Appl. Crystallogr.* **2001**, *34*, 210−213.
(61) Gualtieri, A. F.; Gatta, G. D.; Arletti, R.; Artioli, G.; Ballirano, P.; Cruciani, G.; Guagliardi, A.; Malferrari, D.; Masciocchi, N.; Scardi, P. Quantitative Phase Analysis Using the Rietveld Method: Towards a Procedure for Checking the Reliability and Quality of the Results. *Period. Mineral.* **2019**, *88*, 147−151.
(62) Bernini, F.; Castellini, E.; Malferrari, D.; Castro, G. R.; Sainz Díaz, C. I.; Brigatti, M. F.; Borsari, M. Effective and Selective Trapping of Volatile Organic Sulfur Derivatives by Montmorillonite Intercalated with a μ-Oxo Fe(III). Phenanthroline Complex. *ACS Appl. Mater. Interfaces* **2017**, *9*, 1045−1056.
(63) Mitsuda, T.; Taylor, H. F. W. Influence of Aluminium on the Conversion of Calcium Silicate Hydrate Gels into 11 Å Tobermorite at 90°C and 120°C. *Cem. Concr. Res.* **1975**, *5*, 203−209.

https://doi.org/10.1021/acsomega.1c04193
ACS Omega 2022, 7, 1694−1702

(64) Yamazaki, S.; Toraya, H. Determination of Positions of Zeolitic Calcium Atoms and Water Molecules in Hydrothermally Formed Aluminum-Substiqtuted Tobermorite-1.1nm Using Synchrotron Radiation Powder Diffraction Data. *J. Am. Ceram. Soc.* **2001**, *84*, 2685−2690.
(65) De Villiers, J. P. R. Crystal Structures of Aragonite, Strontianite, and Witherite. *Am. Mineral.* **1971**, *56*, 758−767.
(66) Sitepu, H. Texture and Structural Refinement Using Neutron Diffraction Data from Molybdite (MoO3) and Calcite (CaCO3) Powders and a Ni-Rich Ni50.7Ti49.30 Alloy. *Powder Diffr.* **2009**, *24*, 315−326.
(67) Bonaccorsi, E.; Merlino, S. Modular Microporous Minerals: Cancrinite-Davyne Group and C-S-H Phases. *Rev. Mineral. Geochem.* **2005**, *57*, 241−290.
(68) Sakiyama, M.; Maeshima, T.; Mitsuda, T. Synthesis and Crystal Chemistry of AI-Substituted 11 Å Tobermorite. *J. Soc. Inorg. Mater., Jpn.* **2000**, *7*, 413−419.
(69) Biagioni, C.; Bonaccorsi, E.; Lezzerini, M.; Merlini, M.; Merlino, S. Thermal Behaviour of Tobermorite from N'Chwaning II Mine (Kalahari Manganese Field, Republic of South Africa). I. Thermo-Gravimetric and X-Ray Diffraction Studies. *Eur. J. Mineral.* **2012**, *24*, 981−989.
(70) Ikeda, Y.; Yasuike, Y.; Kumagai, M.; Park, Y.-Y.; Harada, M.; Tomiyasu, H.; Takashima, Y. ^{29}Si MAS NMR Study on Structural Change of Silicate Anions with Carbonation of Synthetic 11Å Tobermorite. *J. Ceram. Soc. Jpn.* **1992**, *100*, 1098−1102.
(71) Galvánková, L.; Másilko, J.; Solný, T.; Štěpánková, E. Tobermorite Synthesis Under Hydrothermal Conditions. *Procedia Eng.* **2016**, *151*, 100−107.
(72) Majdinasab, A.; Yuan, Q. Synthesis of Al-Substituted 11Å Tobermorite Using Waste Glass Cullet: A Study on the Microstructure. *Mater. Chem. Phys.* **2020**, *250*, 123069.
(73) Schreiner, J.; Goetz-Neunhoeffer, F.; Neubauer, J.; Jansen, D. Hydrothermal Synthesis of 11 Å Tobermorite − Effect of Adding Metakaolin to the Basic Compound. *Appl. Clay Sci.* **2020**, *185*, 105432.
(74) Liang, X.; Zang, Y.; Xu, Y.; Tan, X.; Hou, W.; Wang, L.; Sun, Y. Sorption of Metal Cations on Layered Double Hydroxides. *Colloids Surf., A* **2013**, *433*, 122−131.
(75) Sun, H.; Heo, Y.-J.; Park, J.-H.; Rhee, K. Y.; Park, S.-J. Advances in Layered Double Hydroxide-Based Ternary Nanocomposites for Photocatalysis of Contaminants in Water. *Nanotechnol. Rev.* **2020**, *9*, 1381−1396.
(76) Miyake, M.; Komarneni, S.; Roy, R. Kinetics, Equilibria and Thermodynamics of Ion Exchange in Substituted Tobermorites. *Mater. Res. Bull.* **1989**, *24*, 311−320.
(77) Markovska, I.; Mihalev, T.; Sotirova, E. Determination of the Order of Selective Adsorption of Heavy Metals by Natural Zeolite Type Clinoptilolite and Synthetic Clinoptilolite Type L. *J. Balk. Tribol. Assoc.* **2017**, *23*, 376−384.
(78) Li, Y.; Bai, P.; Yan, Y.; Yan, W.; Shi, W.; Xu, R. Removal of Zn2+, Pb2+, Cd2+, and Cu2+ from Aqueous Solution by Synthetic Clinoptilolite. *Microporous Mesoporous Mater.* **2019**, *273*, 203−211.
(79) Malferrari, D.; Brigatti, M. F.; Laurora, A.; Pini, S.; Medici, L. Sorption Kinetics and Chemical Forms of Cd(II) Sorbed by Thiol-Functionalized 2:1 Clay Minerals. *J. Hazard. Mater.* **2007**, *143*, 73−81.
(80) Borden, D. Baseline Studies of the Clay Minerals Society Source Clays: Cation Exchange Capacity Measurements by the Ammonia-Electrode Method. *Clays Clay Miner.* **2001**, *49*, 444−445.
(81) Castellini, E.; Malferrari, D.; Bernini, F.; Franca Brigatti, M.; Rafael Castro, G.; Medici, L.; Mucci, A.; Borsari, M. Baseline Studies of the Clay Minerals Society Source Clay Montmorillonite Stx-1b. *Clays Clay Miner.* **2017**, *65*, 220−233.
(82) Malferrari, D.; Laurora, A.; Brigatti, M. F.; Coltorti, M.; Di Giuseppe, D.; Faccini, B.; Passaglia, E.; Vezzalini, M. G. Open-Field Experimentation of an Innovative and Integrated Zeolitite Cycle: Project Definition and Material Characterization. *Rendiconti Lincei.* **2013**, *24*, 141−150.

https://doi.org/10.1021/acsomega.1c04193
ACS Omega 2022, 7, 1694−1702